Food and Chemical Toxicology 139 (2020) 111260

Contents lists available at ScienceDirect

Food and Chemical Toxicology

journal homepage: www.elsevier.com/locate/foodchemtox

The gut microbiota metabolite urolithin A, but not other relevant urolithins, induces p53-dependent cellular senescence in human colon cancer cells

Juan Antonio Giménez-Bastida, María Ángeles Ávila-Gálvez, Juan Carlos Espín*, Antonio González-Sarrías*

Laboratory of Food and Health, Research Group on Quality, Safety and Bioactivity of Plant Foods, Dept. Food Science and Technology, CEBAS-CSIC, P.O. Box 164, 30100, Campus de Espinardo, Murcia, Spain

ARTICLE INFO

Keywords:
Urolithins
Colon cancer
Cellular senescence
Phase-II metabolism
ABC transporters

ABSTRACT

The promotion of senescence in cancer cells by dietary (poly)phenols gained attention as a promising chemopreventive strategy against colorectal (CRC) and other cancers. Urolithins (Uros) are ellagitannins and ellagic acid-derived gut microbiota metabolites that reach high concentrations in the human colon. They were postulated to be as potential anticancer agents in different CRC models, but their role as promoters of cellular senescence has never been comprehensively evaluated.

We evaluated long-term senescent-mediated chemoprevention of physiologically relevant doses of different Uros and representative mixtures of human urolithin metabotypes in human CRC (HCT-116, Caco-2, and HT-29) and non-tumorigenic (CCD18-Co) cell lines. Our results show that Uro-A (but not Uro-C, IsoUro-A, or Uro-B) leads to a dose-dependent anti-clonogenic effect through the increase of the senescence-associated β–galactosidase activity, rather than by reversible cell cycle arrest and(or) apoptosis which require much higher concentrations. Senescence was accompanied by an elevated p53 and $p21^{Cip1/Waf1}$ expression in HCT-116 cells (p53-wild type), but not in other CRC lines with p53 mutated or non-tumorigenic cells, which suggests that long-term senescence-mediated chemoprevention is a p53-dependent manner. Moreover, the ATP-binding cassette transporters and the phase-II metabolism of Uros limited the induction of senescence, which anticipates lower effects of conjugated Uros against systemic cancers.

1. Introduction

Colorectal cancer (CRC) is one of the most common malignancies (per incidence), and the second cause of cancer-related death worldwide in both sexes (Bray et al., 2018). Early diagnosis and the promotion of healthy dietary habits have been established as essential measures of primary prevention for CRC development (Shike, 1999; Magalhaes et al., 2012; Grosso et al., 2017). Epidemiological studies have described the inverse correlation between CRC incidence and a high intake of fruits and vegetables rich in phytochemicals, including phenolic compounds (Turati et al., 2015; Bingham et al., 2003). However, despite the abundant preclinical (*in vitro* and animal models) anticarcinogenic activity reported for different individual phenolics and phenolic-rich plant foods, the clinical evidence remains elusive so far (Núñez-Sánchez et al., 2015).

Ellagitannins (ETs) and ellagic acid (EA) are polyphenols occurring in pomegranate, walnuts, and many berries. ETs are not absorbed, and EA shows low bioavailability mainly due to its limited solubility under physiological conditions (González-Sarrías et al., 2015). Consequently, EA is metabolized by the colonic microbiota producing a family of bioavailable metabolites known as urolithins (Uros) (Cerdá et al., 2004; Tomás-Barberán et al., 2017). Remarkably, Uros reach relevant concentrations in the lumen and colonic tissues (malignant and normal) of CRC patients after the intake of an ET-rich pomegranate extract (Núñez-Sánchez et al., 2014).

The gut microbiota composition in humans differentially determines the molecular form, concentration, and bioactivity of Uros. This dissimilar metabolism is linked to the inter-individual variability of the human gut microbiota, which has led to identify three different urolithin metabotypes (UMs), i.e., metabotype A (UM-A) where only urolithin A (Uro-A) is the final urolithin produced, metabotype B (UM-B) that produces Uro-A, isourolithin A (IsoUro-A) and urolithin B (Uro-B), and metabotype 0 (UM-0) that does not produce these final Uros (Tomás-Barberán et al., 2014; Romo-Vaquero et al., 2019).

Uros have been extensively studied in CRC models, showing cell cycle arrest and apoptosis induction via modulation of genes and

* Corresponding authors.
E-mail addresses: jcespin@cebas.csic.es (J.C. Espín), agsarrias@cebas.csic.es (A. González-Sarrías).

https://doi.org/10.1016/j.fct.2020.111260
Received 21 December 2019; Received in revised form 6 March 2020; Accepted 10 March 2020
Available online 13 March 2020

Abbreviations

ABC	ATP-binding cassette
ATCC	American type culture collection
CRC	Colorectal Cancer
CV	cristal violet
DMSO	Dimethyl sulfoxide
EA	Ellagic acid
ETs	Ellagitannins
FDG	fluorescein di β-D-galactopyranoside
IsoUro-A	Isourolithin A
LC	Liquid chromatography
MeOH	Methanol
MS	Mass spectrometry
MTT	(3-(4,5-dimethylthiazol-2-yl)-2,5-diphenyltetrazolium bromide)
PBS	Phosphate buffered saline
Uro	Urolithin;
UMs	Urolithin metabotypes

proteins expression, as well as signaling events associated with CRC development (González-Sarrías et al., 2009, 2014, 2016, 2017). However, Uros' activity can vary depending on the cell type and dosage. Besides, their action has only been reported in short-term treatments and thus, we hypothesize that Uros may promote cellular senescence after long-term incubation times.

Cellular senescence has been proposed to be an anticancer mechanism since it prevents irreversible, permanent cell cycle progression on cancer cells accompanied by changes in cell morphology and activation of senescence-associated β-galactosidase (SA-β-gal) as the most common hallmarks. Besides, senescence activation is accompanied by substantial molecular changes in gene expression linked to cell growth inhibition, such as up-regulation of p53, cell cycle inhibitors, including $p21^{Cip1/Waf1}$ and $p16^{INK4a}$, as well as the hypo-phosphorylated form of retinoblastoma (Rb) (Campisi and d'Adda di Fagagna, 2007; Sikora et al., 2011; Muñoz-Espín and Serrano, 2014; Lessard et al., 2018).

To date, only one clinical trial in CRC patients reported some molecular changes in several key CRC-related genes and microRNAs in normal and cancerous colon tissues, after the intake of an ET-rich pomegranate extract (Núñez-Sánchez et al., 2015, 2017). However, the short-term intake (days) disallowed the association of molecular changes with the patients' Uros and (or) EA levels detected in the colon tissues, which prevented possible clinical evidence of Uros against CRC.

The present study aims to investigate whether a panel of Uros and representative mixtures of UMs at physiologically relevant, but non-cytotoxic concentrations can induce senescence in human CRC and non-tumorigenic cells. Additionally, we investigated whether the cellular senescence induction was directly promoted via ATP-binding cassette (ABC) transporters, as well as whether the phase-II metabolism of Uros could limit their effect.

2. Materials and methods

2.1. Reagents

Uro-A, Uro-B, IsoUro-A, and Uro-A sulphate (Uro-A sulph) were obtained from Villapharma Research S.L. (Parque Tecnológico de Fuente Alamo, Murcia, Spain). Uro-C was purchased from Dalton Pharma Services (Toronto, Canada). Urolithin A glucuronide (Uro-A glur) was prepared according to Giménez-Bastida et al. (2012). Purity was higher than 95% for all compounds (Fig. 1). EA, MTT (3-(4,5-dimethylthiazol-2-yl)-2,5-diphenyltetrazolium bromide), propidium iodide, RNase, fluorescein free acid and fluorescein di β-D-galactopyranoside (FDG), crystal violet (CV), Ko143 (Ko), CP100356 (Cp), and probenecid (Prob) were purchased from Sigma-Aldrich (St. Louis, MO, USA). Phosphate buffered saline (PBS), dimethyl sulfoxide (DMSO), methanol (MeOH), acetic acid, and glutaraldehyde were obtained from Fisher Scientific (USA), and DMSO from Panreac (Barcelona, Spain). Ultrapure Millipore water was used throughout the study.

2.2. Cell lines, cell culture conditions, and treatments

The cell lines used in this study were obtained from the American Type Culture Collection (ATCC, Rockville, USA) and cultured as recommended by the ATCC. Human colon cancer cell lines Caco-2 (p53-null) and HT-29 (mutant p53) and non-tumorigenic colon cells CCD18-Co (wild type p53) were grown as reported elsewhere (González-Sarrías et al., 2016). Human colon cancer HCT-116 cells (wild type p53) were grown as previously described (González-Sarrías et al., 2013a). CCD18-Co cells, at population doubling levels between 24 and 34, were used for all experiments.

All tested compounds were solubilized in DMSO (< 0.5% in the culture medium) and filter sterilised (0.2 μm) before addition to the culture media. The cells were treated with DMSO (0.5% v/v; control cells) or EA and Uros (Uro-A, Uro-B, Uro-C, and IsoUro-A) at

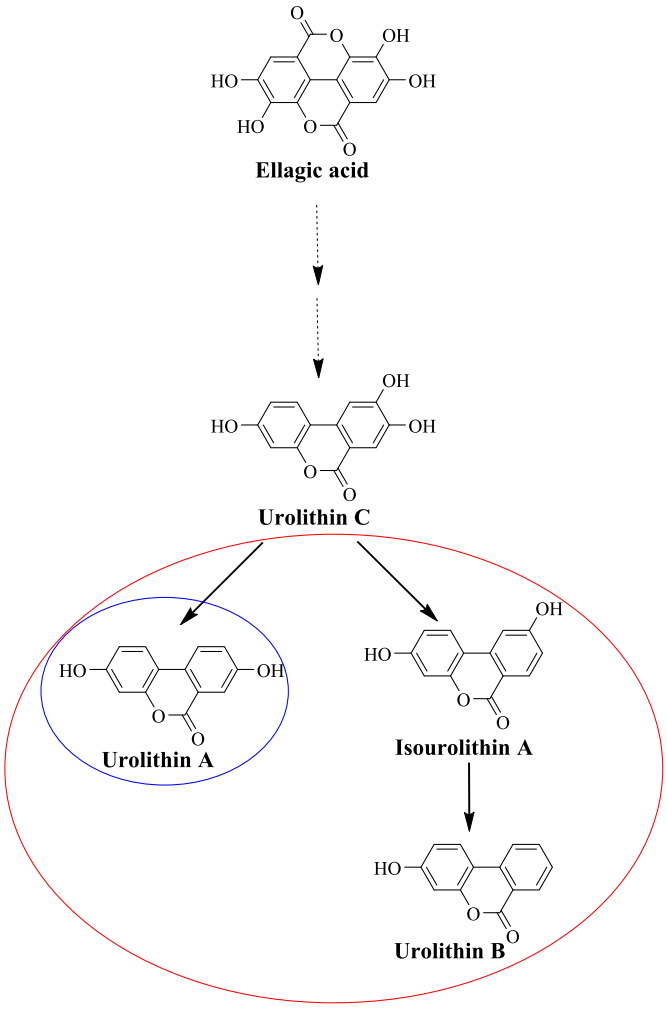

Fig. 1. Ellagic acid (EA), and derived urolithins (Uros) assayed in the present study. The red circle designates the Uros present in UM-B and the blue circle in UM-A. (For interpretation of the references to color in this figure legend, the reader is referred to the Web version of this article.)

physiologically relevant non-cytotoxic concentrations (0.5, 1 and (or) 10 μM). In addition, representative mixtures of Uros, mimicking *in vivo* UMs (metabotype A, UM-A: 80% Uro-A + 20% Uro-C; metabotype B, UM-B: 50% IsoUro-A + 20% Uro-B + 20% Uro-A + 10% Uro-C) (Núñez-Sánchez et al., 2014, 2016; Romo-Vaquero et al., 2015) were also assayed to evaluate a possible synergistic, additive or antagonistic effect. The experiments were carried out at different times of treatment, depending on each specific assay (see below).

Cell concentration was determined using a TC10™ automated cell counter (Bio-Rad, Madrid, Spain), and plated at 6×10^3 (CCD18-Co), and 1.5×10^4 (Caco-2, HT-29 and HCT-116) cells/cm^2 and allowed to grow for 48 h before the treatments.

2.3. Cell viability assay

The effect of EA, Uros (10 μM), and representative mixtures (UM-A and UM-B) on cell viability and proliferation were measured by the MTT reduction assay and CV methods according to Giménez-Bastida et al. (2019). The assays were performed at least in triplicate (n = 3). Each treatment was performed 6 times (6 wells per treatment).

2.4. Clonogenic assays

The cells were seeded at 100 (HCT-116) or 200 cells/well (Caco-2, HT-29, and CCD18-Co) in 12-well plates, incubated for 48 h, and treated with EA, Uros and the mixtures (0.5, 1, and 10 μM) for 14 days. Every 4 days, the culture medium was replaced by fresh-medium containing the treatments. At the end of the treatments, the colonies were fixed with the Carnoy solution, followed by staining with 0.1% CV. The quantification and analysis of colonies formation were performed as described by Guzmán et al. (2014). Data were shown as the average ± SD of 3–5 independent experiments.

2.5. Cell cycle analysis

The effect of EA, Uros, and their mixtures (at 10 μM) on cell cycle distribution was evaluated through DNA content (25,000 cells for each treatment) using a FACScan instrument equipped with FACStation running Cell Quest software (Becton Dickinson, New Jersey, USA) and were carried out as described previously (González-Sarrías et al., 2017). Percentage of cells in G_0/G_1, S, and G_2/M phases, as well as the coefficient of variation (< 5%), were determined using the ModFit LT Version 4.1 acquisition software package (Verity Software House, Topsham, ME, USA). The assays were performed in triplicate and repeated three times. In each independent assay, the cells were treated in duplicate (2 wells per treatment).

2.6. Senescence-associated β-galactosidase (SA-β-gal) assays

The β-Gal activity was determined using the FDG method as described elsewhere (Debacq-Chainiaux et al., 2009; Ortiz-Espín et al., 2017). Briefly, 1000 cells/well were seeded in 96-well plates and incubated for 48 h before treatments. After treatments, cells were fixed and incubated in the dark with a reaction solution containing FDG. Next, 50 μL fluorescein free acid (used as standard curve) and (or) the samples' supernatants were transferred to a black 96-well plate to measure the conversion of FDG to fluorescein (as a result of the β-Gal activity) measured using a fluorescence microplate reader (FLUOstar Omega, BMG Labtech, Ortenberg, Germany) at 485 nm excitation and 520 nm emission. At the end of the assay, to avoid any interference that may cause cytotoxicity or proliferation alteration, cell density was measured by the CV method assay (Feoktistova et al., 2016). Analyses were done at least from 3 to 5 different experiments. In each independent assay, the cells were treated 6 times (6 wells per treatment) for each time point (1, 3, and 5 days).

We considered the results obtained in this assay to explore whether the senescence induced by Uros could be mediated by binding to ATP-binding cassette (ABC) transporters. Thus, the SA-β-Gal activity induction by Uros (10 μM) was evaluated using the FDG method in the presence of a selective ABC transporter inhibitors (a P-gp inhibitor, CP100356 (1 μM)), a BCRP inhibitor, Ko143 (1 μM), and a MRP inhibitor, probenecid (1 μM), respectively, after 5 days of incubation. This assay was repeated three times (n = 3). Each treatment was repeated 6 times (6 wells per treatment).

The estimation of SA-β-gal activity was also performed using a senescence cells staining kit according to the manufacturer's instructions. Briefly, the cells were seeded at 6×10^3 (HT-29), 4×10^3 (CCD18-Co), 3×10^3 (Caco-2), and 1.5×10^3 (HCT-116) cells/cm^2, incubated at 37 °C for 48 h, and then treated at 10 μM for 5 days. Next, the subconfluent cells were washed with PBS, fixed and incubated with the X-Gal staining mixture for 8–12 h (depending on the cell line). Each well was randomly photographed (4–5 pictures at 10 x magnification) using a charge-coupled device (CCD) camera coupled to a contrast inverted microscope. The β-gal activity was determined using the ImageJ 1.52a software (National Institutes of Health, Bethesda, Maryland, USA). The data were displayed as the percentage of the blue-stained area in senescent cells/total cell area from three different replicates (n = 3).

2.7. Western-blot analyses

Based on the senescence results, human colon cancer cells were treated for 5 days at 10 μM. To prepare the whole-cell protein extract, cells were washed twice with ice-cold PBS and scraped in cold RIPA buffer containing protease (Roche, Mannheim, Germany) and phosphatase (1 mM sodium fluoride and 1 mM sodium orthovanadate) inhibitor cocktails. Protein concentration was determined using DC protein assay kit (Bio-Rad, Madrid, Spain). Equal protein amounts (20 μg protein/lane) were loaded and separated in 10–12% SDS-PAGE gels and transferred to nitrocellulose membranes (GE Healthcare, Buckinghamshire, UK). The membranes were incubated overnight with the primary antibodies (Cell Signalling, MA, USA) p53 (1:1000), $p16^{INK4a}$ (1:1000), $p21^{Cip1/Waf1}$ (1:500), glyceraldehyde-3-phosphate dehydrogenase (GAPDH) (1:2500), phospho-Rb (pRb) (1:1000) and total-Rb (tRb) (1:1000), followed by incubation with anti-mouse or anti-rabbit horseradish peroxidase (HRP)-linked secondary antibodies (1:3000). Protein expression was detected using ECL 2 Western Blotting Substrate or SuperSignal West Pico PLUS Chemiluminescent Substrate detection system (ThermoFisher, Barcelona, Spain) according to the manufacturer's instructions, and further analysed in an Amersham Imager 600 (GE Healthcare, Barcelona, Spain). Western blot analyses were done at least in triplicate (n = 3).

2.8. Assessment of phase-II metabolism and stability of urolithins in colon cancer cells

To determine the stability and metabolism of urolithins by human colon cell lines, cell culture supernatants were collected during the treatments (0, 3 and 5 days), processed, and analysed by LC-MS system (1200 Series, Agilent Technologies, Madrid, Spain) as previously described (González-Sarrías et al., 2013b, 2017).

2.9. Statistical analysis

Data were expressed as the mean ± standard deviation (SD). Normal distributed data were analysed by ANOVA followed by Dunnet *post-hoc* test. Figures and graphs were performed using ChemDraw Professional v. 16.0.1.4 (Perkin Elmer Informatics Inc., Cambridge, MA, USA) and Sigma Plot 13.0 (Systat Software, San Jose, CA, USA), respectively. A value of $p < 0.05$ was considered to be statistically significant.

3. Results

3.1. Effect of urolithins on cell cytotoxicity, proliferation and clonogenic growth

Cell viability of the three CRC cell lines (HCT-116, Caco-2, and HT-29) and the non-tumorigenic colon CCD18-Co cells was always above 90% (similar to control cells) in the presence of EA, Uros (Uro-A, -B, -C, and IsoUro-A) and the UMs (10 μM; 5 days), indicating the absence of cytotoxicity (data not shown).

To test whether longer exposure times affected the clonogenic growth, we also treated all colon cell lines with EA, Uros, as well as UMs at non-cytotoxic concentrations (0.5, 1, and 10 μM) for 2 weeks. Uro-A, UM-A, and UM-B, at 10 μM, exerted a significant reduction ($p < 0.05$) in colony formation (57%, 47%, and 35%, respectively) in the HCT-116 cells, whereas this effect was absent at 0.5 and 1 μM (Fig. 2A and B; Supplementary Fig. S1).

Caco-2 cells treated with Uros showed a significant ($p < 0.05$) dose-dependent decrease in the colony formation capacity compared to the DMSO-treated cells (Fig. 3A and B; Supplementary Fig. S2). Uro-A was the most active molecule reducing the clonogenic growth at 10 (61%; $p < 0.05$) and 1 μM (44%; $p < 0.05$). Similarly, Caco-2 cells also showed lower clonogenic growth in the presence of Uro-C at 10 (40%; $p < 0.05$) and 1 μM (33%; $p < 0.05$). At the lowest concentration, Uro-A and Uro-C also exerted anti-clonogenic effect (30–33%), but this effect was not significant (Supplementary Fig. S2). UM-A, IsoUro-A, Uro-B, and UM-B also displayed a dose-dependent reduction of the clonogenic growth, although this effect was only significant at 10 μM (47–69%; $p < 0.05$), whereas EA lacked anti-clonogenic effect at the doses tested.

Regarding HT-29 cells, only Uro-A at 10 μM exerted a statistically significant decrease ($p < 0.05$) in colony formation related to the DMSO-treated cells, whereas no anti-clonogenic effect was observed for the rest of treatments (Fig. 4A and B; Supplementary Fig. S3). Furthermore, no effect in colony formation was observed in the non-tumorigenic CCD18-Co cells under our assay conditions (Supplementary Fig. S4).

We next evaluated whether the observed reduction in the clonogenic effect was mediated via cell cycle regulation or senescence induction in HCT-116 and Caco-2. In parallel, despite the near to absent effects, we also run the experiments with HT-29 and non-tumorigenic colon CCD18-Co to explore the differences between the colon cell lines investigated.

3.2. Effect of urolithins on cell cycle

After 5 days of treatment at the highest dose tested (10 μM), cell cycle distribution in all colon cell lines was investigated by flow cytometry. In line with the clonogenic assay data, the cell cycle distribution in HCT-116 and Caco-2 was affected by some Uro treatments (Fig. 5A and B), whereas none of the treatments arrested the cell cycle in HT-29 or CCD18-Co cells (Supplementary Fig. S5).

HCT-116 cell cycle was altered by Uro-A and UM-A treatments as reflected by the significant arrest at the G_2/M phase ($p < 0.05$) concomitant with a decrease in G_0/G_1 and (or) S phases ($p < 0.05$), compared to DMSO-treated cells. Otherwise, IsoUro-A, Uro-C, and UM-B treatments significantly arrested the cycle at phase S concomitant with a decrease in the G_0/G_1 phase ($p < 0.05$), compared to DMSO-treated cells (Fig. 5A). Regarding Caco-2 cells, Uro-A and IsoUro-A (to a lesser extent) significantly increased the cells' percentage in the G_2/M phase ($p < 0.05$). Similarly, UM-A and UM-B also exerted a significant increment of cells in G_2/M phase ($p < 0.05$). Besides, an increase in S and G_2/M phases (not significant) was observed in Uro-C-treated cells (Fig. 5B).

3.3. Effect of urolithins on cellular senescence induction

To precise whether the anti-clonogenic effect, as well as the cell cycle arrest observed after long-term exposure to Uros, was associated with cellular senescence induction, we investigated the SA-β-gal in response to our treatments.

We first determined the SA-β-Gal as a function of the time of treatment (1, 3, and 5 days) with EA and their microbial metabolites. The highest β-Gal activity, compared to the control cells, was observed in HCT-116 cells treated with Uro-A and UM-A at 10 μM (1.33 ± 0.1 –fold and 1.48 ± 0.2; $p < 0.05$, respectively) for 5 days (Supplementary Fig. S6). No cellular senescence induction was observed at the concentrations investigated in Caco-2, HT-29, and CCD18-Co cells after 1, 3, and 5 days of treatment (Supplementary Figs. S7 and S8A). Considering this, we sought to confirm these results in the HCT-116 cell line using a different methodology such as histochemical staining only at 5 days. In parallel, as a negative control, the same treatments (under the same conditions) were performed in the rest of cell lines (which showed lack of SA-β-Gal). The quantification of the blue-stained cells relative to the total number of cells revealed similar results as those obtained with the FDG assays after 5 days of treatment. Thus, Uro-A and UM-A increased the percentage of blue-stained cells compared to DMSO-treated cells (2.0 ± 0.8 and 2.5 ± 1.1, $p < 0.05$) in HCT-116 (Fig. 6). As expected (based on the FDG method's results), no differences were observed in Caco-2, HT-29, and CCD18-Co (Fig. 7; Supplementary Fig. S8B and S9) using the histochemical assay.

3.4. Effect of urolithins on senescence-associated proteins

To identify the molecular mechanism through Uros may induce cellular senescence, we analysed the expression, by Western blot, of well-established senescence-associated molecular markers, including p53, $p21^{Cip1/Waf1}$, and $p16^{INK4a}$, as well as the phosphorylation level of Rb in the three CRC cell lines.

The expression of p53 was significantly increased in the HCT-116 cells (wild type p53) by Uro-A and UM-A treatments (10 μM for 5 days) (2.1 ± 0.4 –fold and 1.8 ± 0.4; $p < 0.05$, respectively)

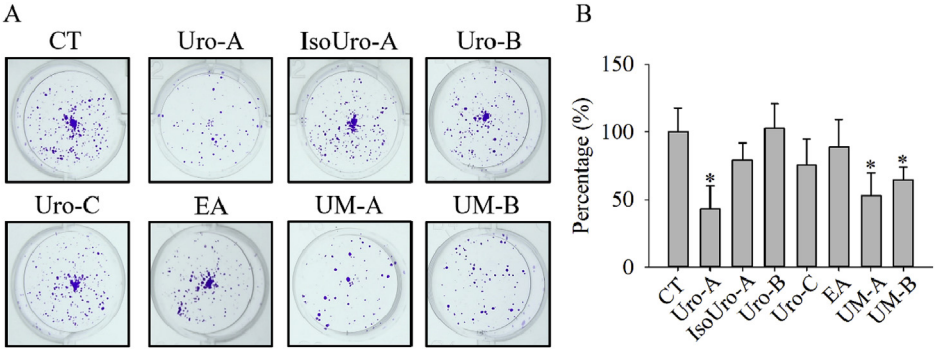

Fig. 2. Anti-clonogenic effect of EA, Uros and UMs (UM-A and UM-B) in HCT-116 cells. A) Illustrative images of the CV-stained HCT-116 cells after the treatment with EA, Uros and UMs (10 μM) for 14 days. B) Quantification of the images using the ColonyArea ImageJ-plugin. The results are showed as the colony intensity percentage (area covered and staining density) compared to the DMSO-treated cells (set as 100%). Values (%) are expressed as the average ± SD (n = 5). *$p < 0.05$.

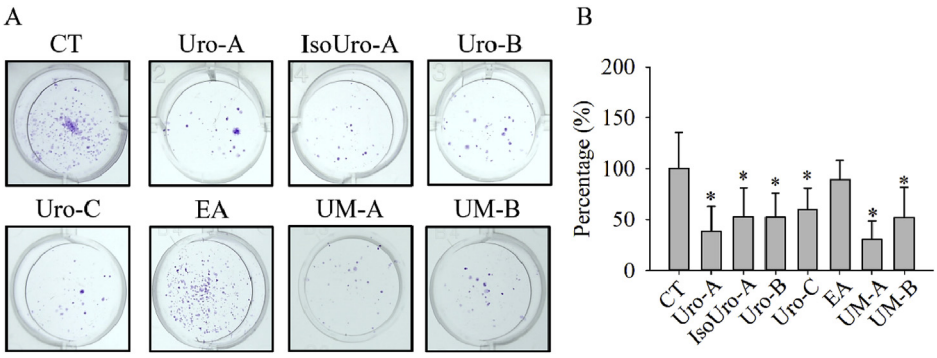

Fig. 3. Anti-clonogenic effect of EA, Uros and UMs (UM-A and UM-B) in Caco-2 cells. A) Illustrative images of the CV-stained Caco-2 cells after the treatment with EA, Uros and UMs (10 μM) for 14 days. B) Quantification of the images was performed as described in Fig. 2. Values (%) are expressed as the average ± SD (n = 4). *$p < 0.05$.

(Fig. 8A). As presented in Fig. 8B, and concomitant with the up-regulation of p53, a significant induction ($p < 0.05$) of the of $p21^{Cip1/Waf1}$ in the cells treated with Uro-A (2.2 ± 0.2) and UM-A (2.2 ± 0.5) was observed. However, the expression level of $p16^{INK4a}$ and the phosphorylation status of Rb obtained was similar to those observed in DMSO-treated cells after all treatments at the dose and time tested (Fig. 8C and D), thus indicating no modulation of the $p16^{INK4a}$/Rb pathway.

On the contrary, for Caco-2 cells (p53-null), none of treatments induced significant changes in p53 protein expression (Fig. 9A) but showed higher expression levels in the treated cells compared to control cells for the cyclin-dependent kinase inhibitor $p21^{Cip1/Waf1}$ reaching statistically significant values for Uro-A, IsoUro-A, and UM-A (1.7 ± 0.3, 1.8 ± 0.4, and 1.8 ± 0.2, respectively; $p < 0.05$) (Fig. 9B). On the other hand, similar to HCT-116 cells, urolithin treatments did not modulate the $p16^{INK4a}$/Rb pathway in Caco-2 cells (Fig. 9C and D).

Finally, as expected, the evaluation in HT-29 cells (mutant p53) of the protein expression of senescence-associated molecular markers and cell cycle reported no effect by none of the treatments compared to control cells (Supplementary Fig. S10).

3.5. Role of ABC transporters and phase-II metabolism in the effect of urolithins on cellular senescence induction

Other mechanisms could mediate cell specificity in senescence induction than p53 modulation, such as differences in phase-II metabolism of Uros in CRC cell lines. Considering this, we evaluated cell metabolism of Uros by all colon cell lines alone and (or) in the presence of ABC transporter inhibitors, at non-toxic concentrations.

The LC-MS analysis of culture medium after incubations with UMs (UM-A and UM-B at 10 μM; Supplementary Fig. S11) for 0, 3, and 5 days revealed that all compounds were stable in the cell media. Regarding cell metabolism, Uros were time-dependent metabolized, via sulphation in HCT-116 or glucuronidation in Caco-2 cells. The HCT-116 cells incubated with UM-A for 5 days formed Uro-A sulph that reached values of 45% (relative to Uro-A), whereas all Uro-C was

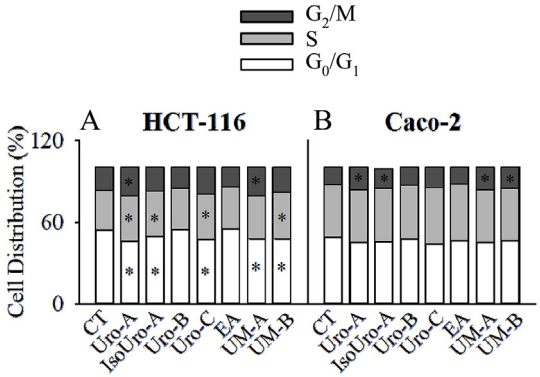

Fig. 5. Effect of EA, Uros and UMs (UM-A and UM-B) on cell cycle distribution. The phases of the cell cycle were quantified using flow cytometry analysis in HCT-116 and Caco-2 cells treated with 10 μM EA, Uros and UMs for 5 days. The stacked bars represent the percentage (mean) of each cell cycle phase in response to each. Cells were treated in duplicate (2 wells per treatment). *$p < 0.05$.

transformed to Uro-C sulph (Supplementary Fig. S11A). Regarding UM-B treatment, data analysis revealed the presence of significant amounts of free Uro-A and IsoUro-A (90% and 45%, respectively) after 5 days of incubation. Remarkably, no conjugated metabolites were observed for Uro-B (Supplementary Fig. S11A).

In Caco-2 cells, a lower cell metabolism of Uros was observed, still detecting amounts of free Uro-A and IsoUro-A of 90% and 45%, respectively, after 5 days of incubation. Remarkably, no conjugated metabolites were observed for Uro-B (Supplementary Fig. S11B).

In the case of HT-29 cells, a complete conjugation of all Uros, mainly glucuronides and in lower amount sulphates, was detected before 5 days (Supplementary Fig. S11C). Finally, no metabolism in any of the Uros incubated with CCD18-Co cells was observed (Supplementary Fig. S11D).

On the other hand, the phase-II conjugation was substantially prevented with the co-incubation of Uros with each ABC transporter

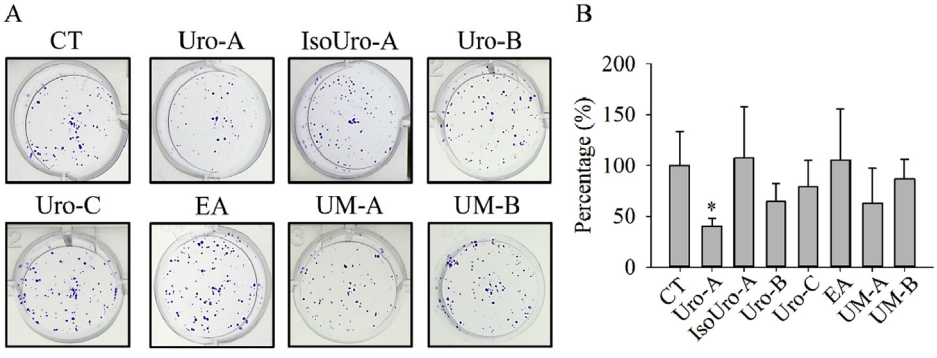

Fig. 4. Anti-clonogenic effect of EA, Uros and UMs (UM-A and UM-B) in HT-29 cells. A) Illustrative images of the CV-stained HT-29 cells after the treatment with EA, Uros and UMs (10 μM) for 14 days. B) Quantification of the images was performed as described in Fig. 2. Values (%) are expressed as the average ± SD (n = 3). *$p < 0.05$.

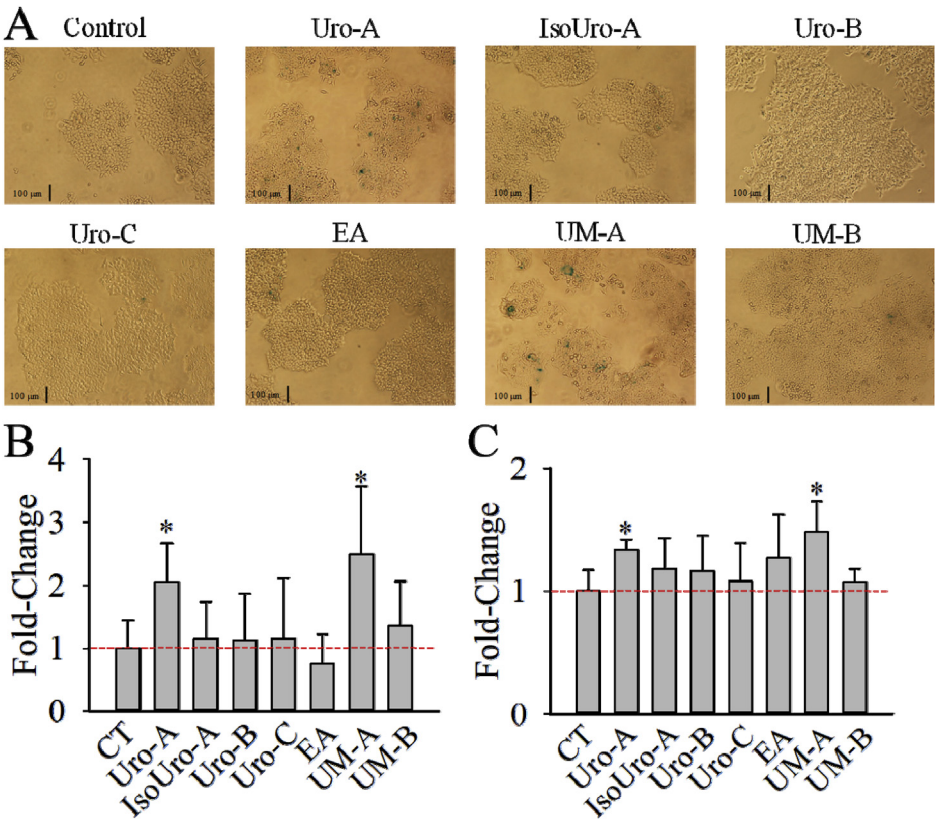

Fig. 6. Effect of EA, Uros and UMs (UM-A and UM-B) on HCT-116 senescence induction. (A) Illustrative images of the HCT-116 cells treated with 10 μM EA, Uros and UMs, followed by the incubation with the staining solution containing X-Gal. (B) Quantification of the pictures showed in (A) and compared to the DMSO-treated cells (set as 1). Values are expressed as the average ± SD (n = 3). (C) Quantification of the SA-β-Gal using the FDG method in response to the different treatments at 10 μM. The red dashed horizontal line shows the control level. Values are expressed as the average ± SD (n = 3; 6 wells per treatment). *$p < 0.05$. (For interpretation of the references to color in this figure legend, the reader is referred to the Web version of this article.)

inhibitor for HCT-116 and Caco-2 cells (Supplementary Figs. S11A–B). Regarding HT-29 cells, no free Uros remained after 3 days of co-incubation (Supplementary Fig. S11C). Notably, the co-treatment with ABC transporter inhibitors plus Uro-A or UM-A (10 μM for 5 days) showed the lack of cellular senescence induction on HCT-116 cells (data not shown), so the entrance into the cells was critical to exert the

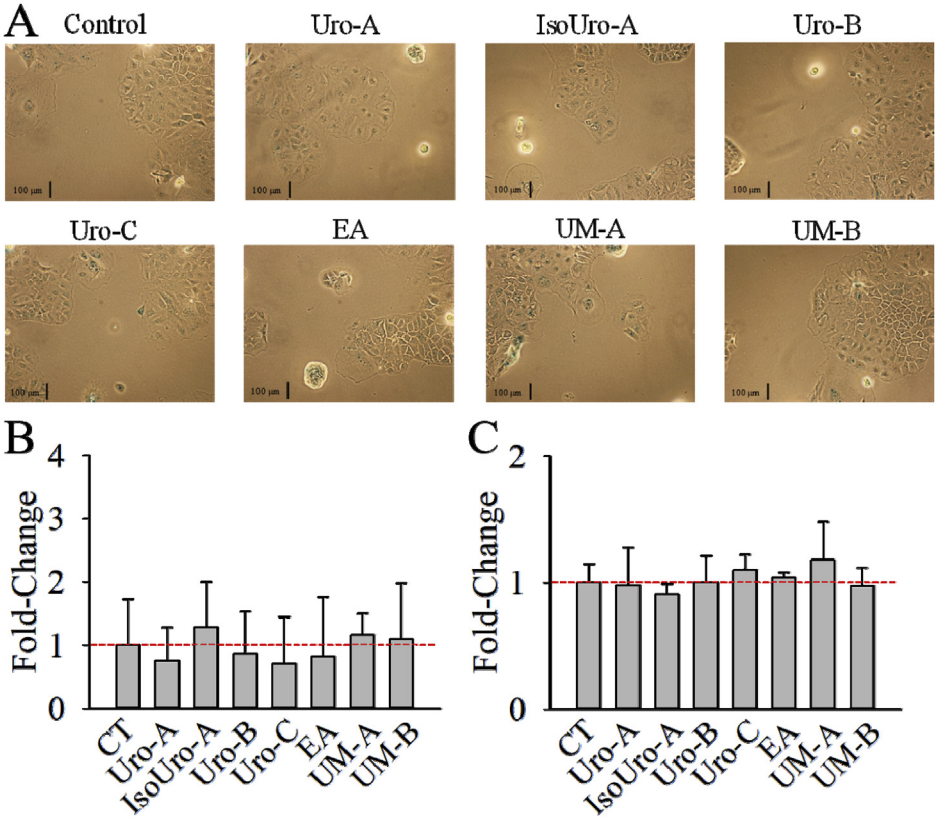

Fig. 7. Effect of EA, Uros and UMs (UM-A and UM-B) on Caco-2 senescence induction. (A) Illustrative images of the Caco-2 cells treated with 10 μM EA, Uros and UMs, followed by the incubation with the staining solution containing X-Gal. (B) Quantification of the pictures showed in (A) and compared to the DMSO-treated cells (set as 1). Values (%) are expressed as the average ± SD (n = 3). (C) Quantification of the SA-β-Gal using the FDG method in response to the different treatments at 10 μM. The red dashed horizontal line shows the control level. Values are expressed as the average ± SD (n = 3; 6 wells per treatment). *$p < 0.05$. (For interpretation of the references to color in this figure legend, the reader is referred to the Web version of this article.)

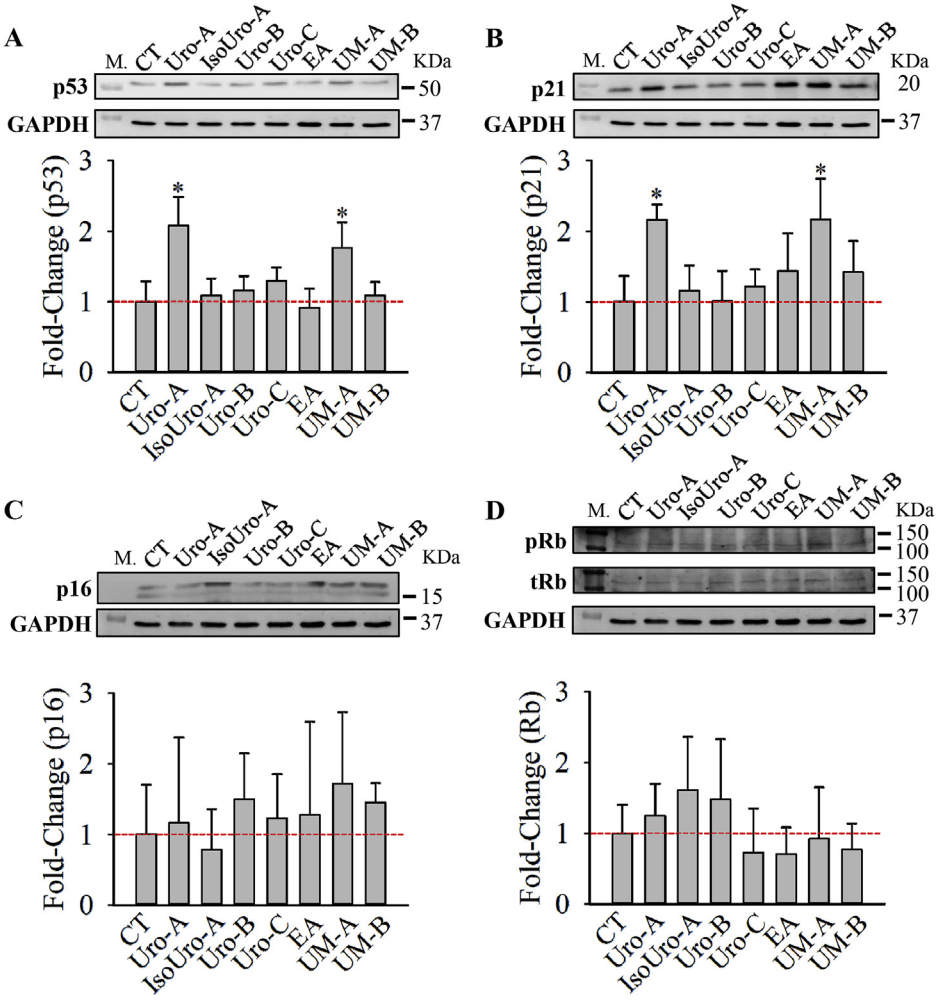

Fig. 8. Determination of (A) p53, (B) p21, (C) p16 as well as the phosphorylation status of (D) Rb, using protein lysates from HCT-166 cells. (pRb and tRb were analysed in different nitrocellulose membranes). GAPDH was used as loading control. The results are expressed as the average ± SD of four different experiments (n = 4). *$p < 0.05$. M, molecular markers.

cellular senescence induction.

To ascertain whether the conversion of free Uros to their conjugated metabolites (choosing as an example the case of Uro-A) limits their effect, we next evaluated the effect of Uro-A glucuronide and Uro-A sulphate (10 μM) on colony formation, as well as cell cycle distribution, and cellular senescence induction after 5 days of treatment against the three different CRC cell lines. However, both Uros conjugates did not exert significant inhibition on cell proliferation nor cellular senescence induction compared to control cells in any of the cell lines used, even on HCT-116 cells (p-53 wild type) (data not shown).

4. Discussion

In the last years, inducing senescence in cancer cells by bioactive compounds such as polyphenols, have gained attention being able to influence tumor development and, therefore, as one of the possible therapeutic approaches to treat cancer (Malavolta et al., 2014; Mária and Ingrid, 2017). This fact is more plausible in the context of CRC since relevant concentrations of polyphenols and (or) derived-metabolites might be reached. Therefore, the interaction with this colon cells can be extensive upon a chronic consumption of certain polyphenols-rich foods.

Numerous studies have demonstrated that the antiproliferative activity of the gut microbial metabolites Uros against different CRC cell lines, being Uro-A the most active molecule compared to the rest of Uros (Núñez-Sánchez et al., 2015; Tomás-Barberán et al., 2017). This is important since Uros reach relevant concentrations in the human colon (Núñez-Sánchez et al., 2014). Although cell cycle arrest and apoptosis induction after short-term assays are among the most acceptable mechanisms for their anticancer effects, the possible contribution of other mechanisms of action to urolithins' chemopreventive effects such as autophagy and cancer cell senescence induction had not been evaluated until recent years.

Submicromolar Uro-A concentrations have been reported to induce autophagy in colon cancer SW620 cells (Zhao et al., 2018), as well as mitophagy in the nematode *C. elegans* after Uro-A treatment (50 μM) (Ryu et al., 2016). However, no effects have been reported on cellular senescence status of nucleus pulposus cells or human skin fibroblasts after low (5–10 μM) and high doses (50 μM) of Uro-A, respectively (Liu et al., 2018, 2019).

In this study, we show that among Uros, only Uro-A, as well as the representative mixture mimicking the urolithin metabotype A (UM-A), have potential to selectively promote cellular senescence against CRC cell lines after long-term exposure. Uro-A exerted dose-dependent anticlonogenic effects via senescence induction, associated with cell cycle arrest at the G_2/M phase in HCT-116 cells, but not in other CRC cell lines (Caco-2 and HT-29) and non-malignant colon cells. This is a significant finding because we demonstrated a new antitumor activity of Uro-A leading to cancer cell senescence, as opposed to reversible cell cycle arrest and (or) apoptosis, which require much higher

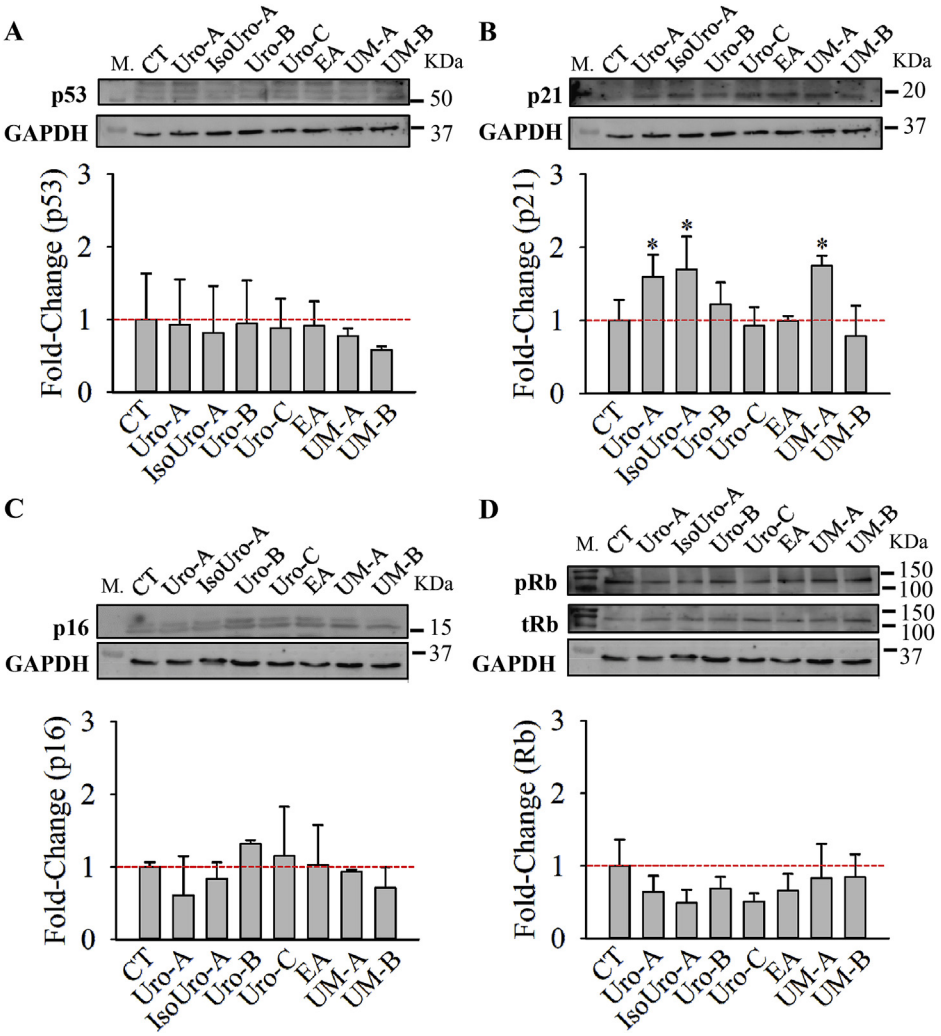

Fig. 9. Determination of (A) p53, (B) p21, (C) p16 as well as the phosphorylation status of (D) Rb, using protein lysates obtained from Caco-2 cells. (pRb and tRb were analysed in different nitrocellulose membranes). GAPDH was used as loading control. The results are expressed as the average ± SD of four different experiments (n = 4). *$p < 0.05$. M, molecular markers.

concentrations. Overall, this suggests a promising chemopreventive strategy against CRC after a regular consumption of ETs-rich foods. Consistent with our data, recent *in vitro* studies reported that long-term treatments with other phenolics such as resveratrol and curcumin have the ability to increase the activity of senescence-associated β-galactosidase (SA-β-gal), and hence, to induce senescence-like growth arrest in human colon cancer HCT-116 and SW620 cells (Heiss et al., 2007; Mosieniak et al., 2012; Colin et al., 2014).

The highest activity of Uro-A on the p53/p21 pathway could be partially related to its OH-moiety at C8 position. This hypothesis aligns with the results of Dirimanov and Högger who described the importance of the OH-group at C8 position for the effect of Uro-A on Akt phosphorylation in endothelial cells (Dirimanov and Högger, 2019). Further evidence is provided by previous studies reporting a reduction of activity of urolithins lacking the OH-group at C8 position, including IsoUro-A and Uro-B (González-Sarrías et al., 2017; Kang et al., 2016).

Regarding UMs, our data might suggest a greater chemopreventive effects in UM-A individuals (Uro-A producers), compared to those with UM-B (Uro-A, IsoUro-A and Uro-B producers). However, the inter-individual variations concerning Uro-A production (i.e., high and low Uros excreters) should be taken into account (Tomás-Barberán et al., 2017). Besides, no apparent synergistic effect was detected in the UM-A mixture. Even so, the lack of effect of EA, clearly points to a low chemopreventive effect in those individuals belong to UM-0 (no Uros producers).

In agreement with previous studies (González-Sarrías et al., 2009, 2014, 2016, 2017), it is important to note that all Uros assayed, except for the UM-B treatment, also exerted dose-dependent anti-clonogenic effects in Caco-2 cells, mediated by a significant cell cycle arrest at G_2/M and S phases, but not by senescence induction. In addition, we also confirmed the lack or lower antiproliferative effect of Uros against HT-29 cells where neither senescence induction was induced. Overall, this fact suggests the possible cellular specificity for the senescence induction by Uro-A.

In this regard, to delve into this possible cellular specificity, we used three different CRC cell lines considering genetic differences, as well as different metabolic characteristics on urolithins. Our data confirmed the highest metabolism of Uros by HT-29, followed by Caco-2, as previously reported (González-Sarrías et al., 2014), as well as the lesser metabolism by HCT-116 cells. Additionally, our data confirmed the lack of induction senescence after Uro-A glucuronide or sulphate treatment compared with their aglycone counterparts in any CRC cell line, similar to that observed in other anticancer activities (González-Sarrías et al., 2014; Ávila-Gálvez et al., 2018). In contrast to conjugated Uro-A metabolites, other conjugated phenolics such as resveratrol (RSV) 3-sulphate and RSV 4′-sulphate were reported to exert induction senescence in HT-29 cells at substantially higher concentrations than those used in the present study (75 μM) (Patel et al., 2013). In terms of relevance to

systemic cancers, our results suggest a possible lower or lack effect on senescence induction of conjugated Uro-A metabolites that can reach systemic tissues *in vivo* (González-Sarrías et al., 2010; Ávila-Gálvez et al., 2019a). Notably, phase-II metabolites from other phenolics such as resveratrol have been reported to induce cellular senescence against breast cancer cells (Giménez-Bastida et al., 2019). Besides, we cannot discard *in situ* deconjugation processes as previously reported for Uro-A glur to Uro-A after lipopolysaccharide (LPS)-induced systemic inflammation in rats (Ávila-Gálvez et al., 2019b). Remarkably, the co-incubation with ABC transporter inhibitors confirmed the reduction of Uros' metabolism previously reported by González-Sarrías et al. (2014), suggesting the essential role of ABC transportes in the transport of Uros into the cell. In this regard, the complete lack of senescence induction exerted by Uro-A in the presence of these inhibitors corroborated that ABC transporters are key factors to facilitate Uro-A effects.

On the other hand, it has been reported that senescence is considered to be a dynamic process that depends on cell types (van Deursen, 2014). Cancer senescent cells frequently possess mutations in two major molecular pathways involved in an irreversible cell cycle arrest and morphological and functional changes, both the tumor suppressor axe p53–p21$^{Cip1/Waf1}$ and pRb-p16^{INK4a} (van Deursen, 2014; Ben-Porath and Weinberg, 2005). Regarding the genetic and molecular mechanisms underlying the Uro-A's senescence-mediated chemopreventive effect, the use of three different CRC cell lines with different p53 expression pattern, that somehow represents colon cancer heterogeneity, has led to demonstrate that Uro-A exerts long-term tumour-senescent chemoprevention in a p53-dependent manner. Thus, our results indicated that the SA-β-galactosidase activation, associated with an upregulation of p53 and p21$^{Cip1/Waf1}$ proteins, was observed only in p53$^{+/+}$ HCT-116 cells, but not in other CRC lines with p53 mutated, after treatment with Uro-A and UM-A. Additionally, a recent evidence reported that Uro-A (at higher concentration that our study, 20 μM) led to p53/p21$^{Cip1/Waf1}$-dependent senescence-like growth arrest at G2/M phase in HCT-116 cells (Norden and Heiss, 2019). Moreover, the data is partly in accordance with previous *in vitro* and *in vivo* studies, in which Uro-A did not induce p53 gene expression in Caco-2 and HT-29 cells even at higher concentration (100 μM) (González-Sarrías et al., 2016), but upregulated its gene expression in the colonic mucosa of rats fed with Uro-A (Larrosa et al., 2010). Moreover, the lack of effect against CCD18-Co normal colon cells that have been reported as wild type p53 could suggest a selective activity towards colon cancer cells compared to normal colon cells. However, the higher growth rate of cancer cells vs. normal cells should not be discarded.

In the same line, the present study also corroborated previous *in vitro* studies that showed Uro-A and other Uros to be able to upregulate the expression of p21$^{Cip1/Waf1}$. These studies reported that this cyclin-dependent kinase inhibitor is involved in the regulation of cell cycle and cell death in Caco-2 cells (González-Sarrías et al., 2016) as well as in other systemic cells such as different prostate cell lines (Sánchez-González et al., 2016; Mohammed Saleem et al., 2019), suggesting that upregulation of p21$^{Cip1/Waf1}$ can be p53-dependent and p53-independent.

The cellular senescence can also be induced in the absence of p53 through a p16/pRb pathway (Takahashi et al., 2006). However, in the present study, both the induction of p16 and the activation of hypophosphorylation of Rb to inhibit cell cycle were not affected by any Uro treatment in any CRC cell line tested, which suggests that cellular senescence induction did not interplay by this senescence-inducing pathway.

Taken together, these findings demonstrate that long-term doses of Uro-A, occurring in the human colon lumen, can inhibit CRC cell growth via induction of senescence through a p53-dependent manner. Further, Uro-A and UM-A, but not other colonic Uros, markedly reduced the cell clonogenicity through cell cycle arrest accompanied by an increase of p53 and p21$^{Cip1/Waf1}$ protein levels in HCT-116 cells, whereas no senescence induction was observed in other p53-deficient CRC cell lines tested. We acknowledge that these findings should be taken with caution since the escape from drug-induced senescence arrest has been previously reported by both stress signals and spontaneously. This could trigger a mechanism of tumor relapse as well as increased invasiveness to exhibit an altered gene expression profile (Roberson et al., 2005; Yang et al., 2017). Collectively these results highlight the significant contribution of senescence induction to Uro-A's anticancer effects.

Funding sources

The study was funded by the projects AGL201564124-R (MINECO, Spain), 201770E081 and 201870I028 (CSIC, Spain). J.A.G.B. is a holder of a Juan de la Cierva contract (IJCI-2016-27633) from the Ministry of Science, Innovation and Universities (Spain).

Author contributions

The authors' responsibilities were as follows: A.G.S. and J.C.E. designed the study; A.G.S., J.A.G.B. and M.A.A.G., performed all experiments and statistical analyses; A.G.S. wrote the manuscript. J.C.E. and J.A.G.B. critically reviewed the manuscript. All authors have read and approved the final manuscript.

CRediT authorship contribution statement

Juan Antonio Giménez-Bastida: Formal analysis, Writing - original draft. **María Ángeles Ávila-Gálvez:** Formal analysis. **Juan Carlos Espín:** Writing - review & editing. **Antonio González-Sarrías:** Formal analysis, Writing - original draft.

Declaration of competing interest

The authors declare that they have no known competing financial interests or personal relationships that could have appeared to influence the work reported in this paper.

Appendix A. Supplementary data

Supplementary data to this article can be found online at https://doi.org/10.1016/j.fct.2020.111260.

References

Ávila-Gálvez, M.Á., Espín, J.C., González-Sarrías, A., 2018. Physiological relevance of the antiproliferative and estrogenic effects of dietary polyphenol aglycones versus their phase-II metabolites on breast cancer cells: a call of caution. J. Agric. Food Chem. 66, 8547–8555.

Ávila-Gálvez, M.Á., García-Villalba, R., Martínez-Díaz, F., Ocaña-Castillo, B., Monedero-Saiz, T., Torrecillas-Sánchez, A., et al., 2019a. Metabolic profiling of dietary polyphenols and methylxanthines in normal and malignant mammary tissues from breast cancer patients. Mol. Nutr. Food Res. 63 e1801239.

Ávila-Gálvez, M.Á., Giménez-Bastida, J.A., González-Sarrías, A., Espín, J.C., 2019b. Tissue deconjugation of urolithin A glucuronide to free urolithin A in systemic inflammation. Food Funct. 10, 3135–3141.

Ben-Porath, I., Weinberg, R.A., 2005. The signals and pathways activating cellular senescence. Int. J. Biochem. Cell Biol. 37, 961–976.

Bingham, S.A., Day, N.E., Luben, R., Ferrari, P., Slimani, N., Norat, T., et al., 2003. Dietary fibre in food and protection against colorectal cancer in the European Prospective Investigation into Cancer and Nutrition (EPIC): an observational study. Lancet 361, 1496–1501.

Bray, F., Ferlay, J., Soerjomataram, I., Siegel, R.L., Torre, L.A., Jemal, A., 2018. Global cancer statistics 2018: GLOBOCAN estimates of incidence and mortality worldwide for 36 cancers in 185 countries. CA A Cancer J. Clin. 68, 394–424.

Campisi, J., d'Adda di Fagagna, F., 2007. Cellular senescence: when bad things happen to good cells. Nat. Rev. Mol. Cell Biol. 8, 729–740.

Cerdá, B., Espín, J.C., Parra, S., Martínez, P., Tomás-Barberán, F.A., 2004. The potent in vitro antioxidant ellagitannins from pomegranate juice are metabolised into bioavailable but poor antioxidant hydroxy-6H-dibenzopyran-6-one derivatives by the colonic microflora of healthy humans. Eur. J. Nutr. 43, 205–220.

Colin, D.J., Limagne, E., Ragot, K., Lizard, G., Ghiringhelli, F., Solary, E., et al., 2014. The role of reactive oxygen species and subsequent DNA-damage response in the

emergence of resistance towards resveratrol in colon cancer models. Cell Death Dis. 5, e1533.
Debacq-Chainiaux, F., Erusalimsky, J.D., Campisi, J., Toussaint, O., 2009. Protocols to detect senescence-associated beta-galactosidase (SA-betagal) activity, a biomarker of senescent cells in culture and in vivo. Nat. Protoc. 4, 1798–1806.
Dirimanov, S., Högger, P., 2019. Screening of inhibitory effects of polyphenols on Akt-phosphorylation in endothelial cells and determination of structure-activity features. Biomolecules 9, 219.
Feoktistova, M., Geserick, P., Leverkus, M., 2016. Crystal Violet Assay for Determining Viability of Cultured Cells Cold Spring Harb Protoc. prot087379.
Giménez-Bastida, J.A., González-Sarrías, A., Larrosa, M., Tomás-Barberán, F., Espín, J.C., García Conesa, M.T., 2012. Ellagitannin metabolites, urolithin A glucuronide and its aglycone urolithin A, ameliorate TNF-a-induced inflammation and associated molecular markers in human aortic endothelial cells. Mol. Nutr. Food Res. 56, 784–796.
Giménez-Bastida, J.A., Ávila-Gálvez, M.Á., Espín, J.C., González-Sarrías, A., 2019. Conjugated physiological resveratrol metabolites induce senescence in breast cancer cells: role of p53/p21 and p16/Rb pathways, and ABC transporters. Mol. Nutr. Food Res. 63, e1900629.
González-Sarrías, A., Espín, J.C., Tomás-Barberán, F.A., García-Conesa, M.T., 2009. Gene expression, cell cycle arrest and MAPK signalling regulation in Caco-2 cells exposed to ellagic acid and its metabolites, urolithins. Mol. Nutr. Food Res. 53, 686–698.
González-Sarrías, A., Giménez-Bastida, J.A., García-Conesa, M.T., Gómez-Sánchez, M.B., García-Talavera, N.V., Gil-Izquierdo, A., et al., 2010. Occurrence of urolithins, gut microbiota ellagic acid metabolites and proliferation markers expression response in the human prostate gland upon consumption of walnuts and pomegranate juice. Mol. Nutr. Food Res. 54, 311–322.
González-Sarrías, A., Ma, H., Edmonds, M.E., Seeram, N.P., 2013a. Maple polyphenols, ginnalins A-C, induce S- and G2/M-cell cycle arrest in colon and breast cancer cells mediated by decreasing cyclins A and D1 levels. Food Chem. 136, 636–642.
González-Sarrías, A., Miguel, V., Merino, G., Lucas, R., Morales, J.C., Tomas-Barberan, F., et al., 2013b. The gut microbiota ellagic acid-derived metabolite urolithin A and its sulfate conjugate are substrates for the drug efflux transporter breast cancer resistance protein (ABCG2/BCRP). J. Agric. Food Chem. 61, 4352–4359.
González-Sarrías, A., Giménez-Bastida, J.A., Núñez-Sánchez, M.A., Larrosa, M., García-Conesa, M.T., Tomás-Barberán, F.A., et al., 2014. Phase-II metabolism limits the antiproliferative activity of urolithins in human colon cancer cells. Eur. J. Nutr. 53, 853–864.
González-Sarrías, A., García-Villalba, R., Núñez-Sánchez, M.Á., Tomé-Carneiro, J., Zafrilla, P., Mulero, J., et al., 2015. Identifying the limits for ellagic acid bioavailability: a crossover pharmacokinetic study in healthy volunteers after consumption of pomegranate extracts. J. Funct. Foods 19, 225–235.
González-Sarrías, A., Núñez-Sánchez, M.A., Tomé-Carneiro, J., Tomás-Barberán, F.A., García-Conesa, M.T., Espín, J.C., 2016. Comprehensive characterization of the effects of ellagic acid and urolithins on colorectal cancer and key-associated molecular hallmarks: MicroRNA cell specific induction of CDKN1A (p21) as a common mechanism involved. Mol. Nutr. Food Res. 60, 701–716.
González-Sarrías, A., Núñez-Sánchez, M.A., García-Villalba, R., Tomás-Barberán, F.A., Espín, J.C., 2017. Antiproliferative activity of the ellagic acid-derived gut microbiota isourolithin A and comparison with its urolithin A isomer: the role of cell metabolism. Eur. J. Nutr. 56, 831–841.
Grosso, G., Bella, F., Godos, J., Sciacca, S., Del Rio, D., Ray, S., et al., 2017. Possible role of diet in cancer: systematic review and multiple meta-analyses of dietary patterns, lifestyle factors, and cancer risk. Nutr. Rev. 75, 405–419.
Guzmán, C., Bagga, M., Kaur, A., Westermarck, J., Abankwa, D., 2014. ColonyArea: an ImageJ plugin to automatically quantify colony formation in clonogenic assays. PloS One 9, e92444.
Heiss, E.H., Schilder, Y.D., Dirsch, V.M., 2007. Chronic treatment with resveratrol induces redox stress- and ataxia telangiectasia-mutated (ATM)-dependent senescence in p53-positive cancer cells. J. Biol. Chem. 282, 26759–26766.
Kang, I., Kim, Y., Tomás-Barberán, F.A., Espín, J.C., Chung, S., 2016. Urolithin A, C, and D, but not iso-urolithin A and urolithin B, attenuate triglyceride accumulation in human cultures of adipocytes and hepatocytes. Mol. Nutr. Food Res. 60, 1129–1138.
Larrosa, M., González-Sarrías, A., Yanez-Gascon, M.J., Selma, M.V., Azorín-Ortuño, M., Toti, S., et al., 2010. Anti-inflammatory properties of a pomegranate extract and its metabolite urolithin-A in a colitis rat model and the effect of colon inflammation on phenolic metabolism. J. Nutr. Biochem. 21, 717–725.
Lessard, F., Igelmann, S., Trahan, C., Huot, G., Saint-Germain, E., Mignacca, L., et al., 2018. Senescence-associated ribosome biogenesis defects contributes to cell cycle arrest through the Rb pathway. Nat. Cell Biol. 20, 789–799.
Liu, H., Kang, H., Song, C., Lei, Z., Li, L., Guo, J., et al., 2018. Urolithin A inhibits the catabolic effect of TNFalpha on nucleus pulposus cell and alleviates intervertebral disc degeneration in vivo. Front. Pharmacol. 9, 1043.
Liu, C.F., Li, X.L., Zhang, Z.L., Qiu, L., Ding, S.X., Xue, J.X., et al., 2019. Antiaging effects of urolithin A on replicative senescent human skin fibroblasts. Rejuvenation Res. 22, 191–200.
Magalhaes, B., Peleteiro, B., Lunet, N., 2012. Dietary patterns and colorectal cancer: systematic review and meta-analysis. Eur. J. Canc. Prev. 21, 15–23.
Malavolta, M., Costarelli, L., Giacconi, R., Piacenza, F., Basso, A., Pierpaoli, E., et al., 2014. Modulators of cellular senescence: mechanisms, promises, and challenges from in vitro studies with dietary bioactive compounds. Nutr. Res. 34, 1017–1035.
Mária, J., Ingrid, Ž., 2017. Effects of bioactive compounds on senescence and components of senescence associated secretory phenotypes in vitro. Food Funct. 8, 2394–2418.
Mohammed Saleem, Y.I., Albassam, H., Selim, M., 2019. Urolithin A induces prostate cancer cell death in p53-dependent and in p53-independent manner. Eur. J. Nutr. https://doi.org/10.1007/s00394-019-02016-2.
Mosieniak, G., Adamowicz, M., Alster, O., Jaskowiak, H., Szczepankiewicz, A.A., Wilczynski, G.M., et al., 2012. Curcumin induces permanent growth arrest of human colon cancer cells: link between senescence and autophagy. Mech. Ageing Dev. 133, 444–455.
Muñoz-Espín, D., Serrano, M., 2014. Cellular senescence: from physiology to pathology. Nat. Rev. Mol. Cell Biol. 15, 482–496.
Norden, E., Heiss, E.H., 2019. Urolithin A gains in antiproliferative capacity by reducing the glycolytic potential via the p53/TIGAR axis in colon cancer cells. Carcinogenesis 40, 93–101.
Núñez-Sánchez, M.A., García-Villalba, R., Monedero-Saiz, T., García-Talavera, N.V., Gómez-Sánchez, M.B., Sánchez-Álvarez, C., et al., 2014. Targeted metabolic profiling of pomegranate polyphenols and urolithins in plasma, urine and colon tissues from colorectal cancer patients. Mol. Nutr. Food Res. 58, 1199–1211.
Núñez-Sánchez, M.A., González-Sarrías, A., Romo-Vaquero, M., García-Villalba, R., Selma, M.V., Tomás-Barberán, F.A., et al., 2015. Dietary phenolics against colorectal cancer–From promising preclinical results to poor translation into clinical trials: pitfalls and future needs. Mol. Nutr. Food Res. 59, 1274–1291.
Núñez-Sánchez, M.A., Karmokar, A., González-Sarrías, A., García-Villalba, R., Tomás-Barberán, F.A., García-Conesa, M.T., et al., 2016. In vivo relevant mixed urolithins and ellagic acid inhibit phenotypic and molecular colon cancer stem cell features: a new potentiality for ellagitannin metabolites against cancer. Food Chem. Toxicol. 92, 8–16.
Núñez-Sánchez, M.A., González-Sarrías, A., García-Villalba, R., Monedero-Saiz, T., García-Talavera, N.V., Gómez-Sánchez, M.B., et al., 2017. Gene expression changes in colon tissues from colorectal cancer patients following the intake of an ellagitannin-containing pomegranate extract: a randomized clinical trial. J. Nutr. Biochem. 42, 126–133.
Ortiz-Espín, A., Morel, E., Juarranz, A., Guerrero, A., González, S., Jiménez, A., et al., 2017. An extract from the plant deschampsia Antarctica protects fibroblasts from senescence induced by hydrogen peroxide. Oxid. Med. Cell. Longev. 2017, 2694945.
Patel, K.R., Andreadi, C., Britton, R.G., Horner-Glister, E., Karmokar, A., Sale, S., et al., 2013. Sulfate metabolites provide an intracellular pool for resveratrol generation and induce autophagy with senescence. Sci. Transl. Med. 5, 205ra133.
Roberson, R.S., Kussick, S.J., Vallieres, E., Chen, S.Y., Wu, D.Y., 2005. Escape from therapy-induced accelerated cellular senescence in p53-null lung cancer cells and in human lung cancers. Canc. Res. 65, 2795–2803.
Romo-Vaquero, M., García-Villalba, R., González-Sarrías, A., Beltrán, D., Tomás-Barberán, F.A., Espín, J.C., et al., 2015. Interindividual variability in the human metabolism of ellagic acid: contribution of Gordonibacter to urolithin production. J. Funct. Foods 17, 785–791.
Romo-Vaquero, M., Cortés-Martín, A., Loria-Kohen, V., Ramírez-de-Molina, A., García-Mantrana, I., Collado, M.C., et al., 2019. Deciphering the human gut microbiome of urolithin metabotypes: association with enterotypes and potential cardiometabolic health implications. Mol. Nutr. Food Res. 63, e1800958.
Ryu, D., Mouchiroud, L., Andreux, P.A., Katsyuba, E., Moullan, N., Nicolet-Dit-Felix, A.A., et al., 2016. Urolithin A induces mitophagy and prolongs lifespan in C. elegans and increases muscle function in rodents. Nat. Med. 22, 879–888.
Sánchez-González, C., Ciudad, C.J., Izquierdo-Pulido, M., Noé, V., 2016. Urolithin A causes p21 up-regulation in prostate cancer cells. Eur. J. Nutr. 55, 1099–1112.
Shike, M., 1999. Diet and lifestyle in the prevention of colorectal cancer: an overview. Am. J. Med. 106 11S-5S; discussion 50S-1S.
Sikora, E., Arendt, T., Bennett, M., Narita, M., 2011. Impact of cellular senescence signature on ageing research. Ageing Res. Rev. 10, 146–152.
Takahashi, A., Ohtani, N., Yamakoshi, K., Iida, S., Tahara, H., Nakayama, K., et al., 2006. Mitogenic signalling and the p16INK4a-Rb pathway cooperate to enforce irreversible cellular senescence. Nat. Cell Biol. 8, 1291–1297.
Tomás-Barberán, F.A., García-Villalba, R., González-Sarrías, A., Selma, M.V., Espín, J.C., 2014. Ellagic acid metabolism by human gut microbiota: consistent observation of three urolithin phenotypes in intervention trials, independent of food source, age, and health status. J. Agric. Food Chem. 62, 6535–6538.
Tomás-Barberán, F.A., González-Sarrías, A., García-Villalba, R., Núñez-Sánchez, M.A., Selma, M.V., García-Conesa, M.T., et al., 2017. Urolithins, the rescue of "old" metabolites to understand a "new" concept: metabotypes as a nexus among phenolic metabolism, microbiota dysbiosis, and host health status. Mol. Nutr. Food Res. 61.
Turati, F., Rossi, M., Pelucchi, C., Levi, F., La Vecchia, C., 2015. Fruit and vegetables and cancer risk: a review of southern European studies. Br. J. Nutr. 113 (Suppl. 2), S102–S110.
van Deursen, J.M., 2014. The role of senescent cells in ageing. Nature 509, 439–446.
Yang, L., Fang, J., Chen, J., 2017. Tumor cell senescence response produces aggressive variants. Cell Death Discov. 3, 17049.
Zhao, W., Shi, F., Guo, Z., Zhao, J., Song, X., Yang, H., 2018. Metabolite of ellagitannins, urolithin A induces autophagy and inhibits metastasis in human sw620 colorectal cancer cells. Mol. Carcinog. 57, 193–200.